FTD-HT-23-1321-68

FOREIGN TECHNOLOGY DIVISION

FUEL BURNUP AND HOT-FLOW MODELING OF COMBUSTION CHAMBERS

By

Ya. P. Storozhuk, V. A. Asoskov

EDITED TRANSLATION

FUEL BURNUP AND HOT-FLOW MODELING OF COMBUSTION CHAMBERS

By: Ya. P. Storozhuk, V. A. Asoskov

English Pages: 35

Source: Leningrad. Tsentral'nyy Nauchno-Issledovatel'skiy I Proyektno-Konstruktorskiy Kotloturbinnyy Institut. Trudy(Leningrad. Central Scientific Research Design Institute of Boilers and Turbines. Transactions 1967, No. 75, pp.110-137

Translated Under: F33657-68-D-0865-P002

DATA HANDLING PAGE

01-ACCESSION NO. 02-DOCUMENT LOC TT9001151	20-TOPIC TAGS combustion chamber, engine combustion system, fuel combustion, combustion chamber temperature, flame tube, scale model
09-TITLE FUEL BURNUP AND HOT-FLOW MODELING OF COMBUSTION CHAMBERS	
07-SUBJECT AREA 21	

12-AUTHOR/CO-AUTHORS STOROZHUK, YA. P. ; 16-ASOSKOV, V. A.	10-DATE OF INFO -----67
03-SOURCE LENINGRAD. TSENTRAL'NYY NAUCHNO-ISSLEDOVATEL'SKIY I PROYEKTNO-KONSTRUKTORSKIY KOTLOTURBINNYY INSTITUT. TRUDY (RUSSIAN) FTD-	08-DOCUMENT NO. HT-23-1321-68
	09-PROJECT NO. 72301-78

05-SECURITY AND DOWNGRADING INFORMATION UNCL, 0			04-CONTROL MARKINGS NONE	07-HEADER CLASN UNCL
06-REEL FRAME NO. 1889 1653	77-SUPERSEDES	78-CHANGES	08-GEOGRAPHICAL AREA UR	NO OF PAGES 35
CONTRACT NO. F33657-68-D-0865-P002	X REF ACC. NO. 65-AT8000505	PUBLISHING DATE 94-	TYPE PRODUCT TRANSLATION	REVISION FREQ NONE
STEP NO. 02-UR/3196/67/000/075/0110/0137			ACCESSION NO.	

ABSTRACT

(U) To simplify the analysis of the combustion process taking place in gas turbines, it is recommended that the process be broken down into simplified stages. In the combustion of a liquid fuel, the process will consist of the following stages: (1) preheating and evaporation of the fuel droplets; (2) the mixing of the atomized fuel and its vapor with air; and (3) the chemical reaction of the fuel vapor with oxygen. In selecting and comparing thermal loads, it is necessary to consider the burnout coefficient, pressure losses, and temperature fields behind the chamber, maximum temperature of the flame tube wall, the combustion stability limits, and the fuel properties. Orig. art. has: 13 figures, 4 tables and 52 formulas.

7. FUEL BURNUP AND HOT-FLOW MODELING OF COMBUSTION CHAMBERS

Ya.P. Storozhuk, V.A. Asoskov

The process of fuel burnup along the combustion chamber length depends on geometric and operating factors (including the chamber diameter, the register construction, the design of the gas discharge openings and their arrangement in the register), on the dispersion of the atomized liquid fuel, the intensity of the mixture formation (air and gas velocities at the exit from the burners), the excess air coefficient, pressure and temperature at which the fuel combustion takes place. Also important are the thermal loadings referred to the chamber volume and cross section, and the chamber hydraulic resistance.

The complexity of the processes which take place in the process of the combustion of liquid and gaseous fuel leads to the necessity for breaking down the over-all process into individual simpler stages. When burning a liquid fuel these stages are:

1) warmup and evaporation of the fuel droplets;

2) mixing of the atomized fuel and its vapors with the air;

3) chemical reactions of the combination of the fuel vapors with oxygen; combustion of gaseous fuel is accomplished in the last two stages only.

This breakdown simplifies the theoretical analysis of the combustion process and permits correlation of experimental data obtained on experimental and industrial combustion chambers.

Comparison of the parameters of existing gas turbine engines [GTE](ГТУ), and also study of experience in their operation shows that in spite of the various geometric and operating conditions, the combustion chambers have a definite range of combustion intensities and hydraulic resistances. Table 2.1 presents the operating characteristics of the combustion chambers of existing GTE or those being readied for production by the Soviet turbine construction plants.

In selecting and comparing combustion intensities we must take into account the combustion completeness coefficient, the pressure losses along the passages, the temperature field at the chamber exit, the values of the maximal temperature of the flame-tube metal, the combustion stability limits and the type of fuel being burned.

We see from Table 2.1 that it is practically impossible to establish any general pattern on the selection of the parameters and the performance achieved. However, for similar combustion completeness coefficients the thermal loads referred to the flame-tube section, which basically determine the burnup completeness, regardless of whether natural gas or liquid fuel is burned, lie in the range $U_F = 5{,}5 \cdot 10^6 - 8{,}5 \cdot 10^6$ kcal/m$^2 \cdot$h$\cdot$atm abs, and the hydraulic resistances lie in the range 1.2-2.6%, with the exception of the ГТ-50-800, high- and low-pressure combustion chambers, whose resistance exceeds the indicated values and amounts to 2.8 and 3.5%.

We note here the important circumstance that increase of the pressure losses in the chamber by 1% leads to a reduction of the GTE specific power on the average by about 1%, and possibly even more, depending on the compression ratio and gas temperature at the turbine inlet. Therefore it is more correct to evaluate the efficiency of the combustion chamber operation not only on the basis of combustion completeness alone, but with account for the hydraulic losses

$$\eta_{к.с} = \eta_т \eta_{гидр}, \qquad (7.1)$$

where η_t is the chamber thermal efficiency;

η_{gidr} is the chamber hydraulic efficiency.

Comparison of the methods for determining the values of the thermal and hydrauli c efficiencies has shown that the best method for determining these quantities is the small deviation method.

$$\eta_т = 100 - k_1 \frac{\Delta T}{T_{з.к}} (100 - \eta_{ст}), \ \%; \qquad (7.2)$$

$$\eta_{гидр} = 100 - k_2 \frac{\Delta P}{P}, \ \%. \qquad (7.3)$$

Here ΔT is the design air temperature rise in the combustion chamber, °K;

$T_{z.k}$ is the turbine inlet (combustor exit) gas temperature, °K;

$\Delta P/P$ are the total pressure losses in the combustion chamber, %;

k_1 is the power loss coefficient due to thermal losses;

k_2 is the power loss coefficient due to hydraulic losses.

The coefficients k_1 and k_2 are determined by the small deviation method for each machine separately and are the percentage power loss per 1% thermal and hydraulic losses, respectively. Thus, for the ГТН-9-750 engine $k_1 = 4{,}9\%$, $k_2 = 1{,}5\%$.

Consequently, in the nominal load regime for $\Delta T = 557°$ K, $T = 1023°$ K, $\frac{\Delta P}{P} = 1{,}7\%$ and $\eta_{cr} = 99{,}5\%$ the combustor efficiency

$$\eta_{k.c} = \left[100 - 4{,}9\,\frac{557}{1023}(100 - 99{,}5)\right](100 - 1{,}5 \cdot 1{,}7) = 96{,}1\%.$$

For the combustors of other gas turbine engines, whose characteristics are presented in Table 2.1, the over-all combustor efficiency will vary in the range 0.92-0.98, depending on the magnitude of the chamber resistance, since the percentage power loss depends not only on the thermal losses, but also on the hydraulic losses.

For acceptable values of the fuel combustion completeness (98-99%), flametube metal temperatures (750-800°C) and hydraulic resistances $\left(\frac{\Delta P}{P} = 1{,}3-2{,}2\%\right)$, depending on the construction of the register it is recommended that the value of the combustion intensity referred to the flametube section be selected in the range $5{,}5 \cdot 10^6 - 6{,}5 \cdot 10^6$ kcal/m^2·h·atm abs. It is recommended that these combustion intensities be used, regardless of the type of fuel burned (liquid fuel and natural gas), since operating experience and the tests conducted have shown that combustion of natural gas does not yield major advantages in comparison with liquid fuel. The selection of larger values of the thermal loading $\sim (7{,}6-8{,}0) \cdot 10^6$ kcal/m^2·h·atm abs than those indicated leads, as in the case of the ГТ-50-800 engine, to a significant increase of the hydraulic losses $\left(\frac{\Delta P}{P} \approx 2{,}8-3{,}5\%\right)$ and high temperatures of the flametube metal. However, it should be noted that if we intensify the process of flametube metal cooling, for example, by transverse ribs, as was done for the ГТ-2,5-1200 chamber, then even with an inlet air temperature of 540°C and an exit temperature 1200°C from the chamber it is possible to obtain an acceptable metal temperature for combustion intensities of $8.4 \cdot 10^6$ kcal/m^2·h·atm abs and $\Delta P/P = 2.3\%$. We see from Table 2.1 that in a combustion chamber of the aviation type used in the ГТ-5 engine made by the Kolomenskiy Plant (and certain other GTE) combustion intensities of $9.0 \cdot 10^6$ kcal/m^2·h·atm abs are realized with resistances $\frac{\Delta P}{P} \approx 2{,}7\%$. We should keep in mind, as indicated previously, that such chambers have comparatively small diameters (200-350 mm), and the metal of the front end of the flametube has high temperatures in these chambers. These chambers require special and careful development, and in spite of this smoke formation and even coking will occur when using the medium and heavy fuels in certain operating regimes.

The length of the burning zone of the combustion chamber in existing GTE (see Table 2.1) lies in the range $\frac{L_{or}}{D_{n.r}} = 1{,}6-2{,}8$, where L_{og} is the flametube length from the burner to the mixer. The burners used for combustion intensities $U_F = 5{,}5 \cdot 10^6 - 6{,}5 \cdot 10^6$ kcal/m^2·h·atm abs, $\alpha_1 = 1{,}2-1{,}4$, $t_s = 200-350$°C, $P = 1{,}5-10$ atm gage and $\frac{\Delta P}{P} = 1{,}3-2{,}2\%$ provide liquid and gaseous fuel burnup to an efficiency of 98-99.5% over the relative lengths indicated above.

It has been found experimentally that the type of register or burner have the greatest influence on the burnup distance in the range of operating parameters listed above. Figure 27 shows the burnup zones for liquid and gaseous fuel along the flametube length

for combustion chambers with plane-conical, conical and semiconical registers, and also gas burners. In plotting the curves we used experimental data obtained on various combustion chambers in the operating parameter range noted above. We see in Fig. 27 that in the forward portion of the chamber the burnup curves for the different chambers spread over quite a broad region and have a different upper limit for the chemical unburned fraction q_{khim}.

For example, over the relative length $L_{or}/D_{n.t}=0,8$ when using conical and semiconical registers and burning liquid fuels the upper limit of $q_{khim} \approx 12\%$, when using plane-conical registers $q_{khim} \approx 20\%$; over this same relative length when burning gaseous fuel using a plane-conical register in the burner $q_{khim} = 40\%$. Toward the rear of the chambers the burnup curves converge. Judging from the burnup curves, the combustion process terminates for combustion chambers with plane-conical registers over a relative length which does not exceed $L_{or}/D_{n.t}=2,0-2,2$, for conical and semiconical registers the relative length is $L_{or}/D_{n.t}=1,7-1,8$ and with gas burners $L_{or}/D_{n.t}=1,9-2,2$. It should be noted that burnup is completed over these distances for normal operation of the spray nozzles and burners, and also for the design air distribution among the chamber passages.

The burnup length may increase if there are any disruptions or deviations in the operation of the chamber elements. Therefore in designing combustion chambers it is desirable to select the length of the burning region (up to the mixer) of the flametube with some margin, depending on the resistances and degree of forcing used: when using plane-conical registers $L_{or}/D_{n.t}=2,3-2,5$; when using conical and semiconical registers $L_{or}/D_{n.t}=2,0-2,2$, and when using gas burners $L_{or}/D_{n.t}=2,0-2,4$.

In the present state of the theory of the combustion chamber working process it is difficult to carry out with the required accuracy the analytic study of the burnup completeness for acceptable geometric dimensions, and also the analytic estimation of the effect of the most important factors on the combustion chamber operating characteristics. In particular, it is not possible to evaluate analytically the effect on the working process in the chamber of the air pressure and temperature, the flow aerodynamic characteristics, the chamber geometrical dimensions and the temperature characteristics of the flametube metal operation. Under these conditions it becomes very important to establish the rules for modeling combustion chambers which will permit conversion of data from a model to full scale and will permit solving questions which are not subject to analysis.

The process of fuel burning under actual combustion chamber conditions is a complex ensemble of heat and mass transfer phenomena in the presence of mass and heat sources and sinks and takes place under conditions of considerable nonuniformity of the gas concentrations, temperatures and velocities. These phenomena are represented by the basic laws of physics: conservation of momentum, mass and energy. These laws are formulated mathematically by differential equations:

1) fluid motion (Navier-Stokes equation)

$$w_x\frac{\partial w_x}{\partial x}+w_r\frac{\partial w_x}{\partial r}=g\left(1-\frac{\partial P}{\partial x}\cdot\frac{1}{\gamma_r}\right)+\nu\left[\left(\frac{\partial^2 w_x}{\partial x^2}+\frac{\partial^2 w_x}{\partial r^2}\right)+\right.$$
$$\left.+\frac{1}{3}\left(\frac{\partial^2 w_x}{\partial x^2}+\frac{\partial^2 w_r}{\partial x\,\partial r}\right)\right]; \qquad (7.4)$$

2) mass transfer in the presence of mass sources and sinks

$$\frac{\partial}{\partial x}\left(D_T\gamma_r\frac{\partial c_n}{\partial x}\right)+\frac{\partial}{\partial r}\left(D_T\gamma_r\frac{\partial c_n}{\partial r}\right)-w_x\gamma_r\frac{\partial c_n}{\partial x}-w_r\gamma_r\frac{\partial c_n}{\partial r}+ \qquad (7.5)$$
$$+W_{\text{исп}}-W_{\text{хим}}=0;$$

3) heat transfer in the presence of heat sources and sinks

$$\frac{\partial}{\partial x}\left(\lambda\frac{\partial T}{\partial x}\right)+\frac{\partial}{\partial r}\left(\lambda\frac{\partial T}{\partial r}\right)-c_p\gamma_r w_x\frac{\partial T}{\partial x}- \qquad (7.6)$$
$$-c_p\gamma_r w_r\frac{\partial T}{\partial r}-q_{\text{исп}}W_{\text{исп}}+q_{\text{хим}}W_{\text{хим}}=0.$$

To determine the concentration, temperature and velocity fields in the chamber volume it is necessary to solve jointly these equations with the corresponding boundary conditions. Since the solution in general form presents considerable difficulties, it is advisable to utilize the similarity method, which permits representing the solution of the system of differential equations in the form of experimental similarity criteria relationships; obtained from the given system.This transformation of the equations (7.4, 7.5 and 7.6) with account for the flow velocity turbulent pulsations yields nine similarity criteria for the combustion process in geometrically similar combustion chambers:

1) the Reynolds criteria, Re=idem;

2) the product of the Mach criterion by the polytropic exponent, Ma k=idem;

3) the Prandtl diffusion criterion, $\text{Pr}_д$=idem;

4) the Prandtl thermal criterion, $\text{Pr}_т$=idem;

5) the turbulence intensity (Karman criterion), Ka=idem;

6) the criterion for the similarity of the temperature and concentration fields,

$$\frac{c_n}{Tc_p}(q_{\text{хим}}-q_{\text{исп}})=\text{idem};$$

experiment [10, 27, 28, 29, 30, 31] shows that this condition is satisfied for the same full-scale and model values of the primary and total excess air, inlet air temperature, fuel flame cone angle, i.e., α_1=idem, $\alpha_{\text{общ}}$=idem, $t_в$=idem, $\beta_ф$=idem;

7) ratio of turbulent mixing time to flow time:

$$\frac{\tau_{см}}{\tau_{пр}} \sim \frac{w_x r^2}{D_т L} = \text{idem}; \qquad (7.7)$$

8) ratio of vaporization time to flowtime:

$$\frac{\tau_{исп}}{\tau_{пр}} \sim \frac{w_x \gamma_г c_п}{W_{исп} L} = \text{idem}; \qquad (7.8)$$

9) ratio of chemical reaction time to flowtime:

$$\frac{\tau_x}{\tau_{пр}} \sim \frac{w_x \gamma_г c_п}{L W_{хим}} = \text{idem}. \qquad (7.9)$$

When burning gaseous fuel the conditions $\beta_\phi = \text{idem}$ and $\frac{\tau_{исп}}{\tau_{пр}} = \text{idem}$ drop out. In practice there is no need to maintain all the similarity criteria listed above the same for flow-scale and the model in simulation, since in the range of variation of the GTE operating parameters and in the region of Re self-similarity, on the basis of experimental data [1, 10, 28, 30, 31, 32] we can consider that the combustion process is independent of the criteria Re, Ka, $Pr_д$, $Pr_т$ and Mak. Then the condition for approximate similarity of the combustion process is written as:

1) geometrical similarity;

2) $\alpha_{общ}$, α_1, β_ϕ, $t_в$ and the fuel must be the same;

3) $\frac{\tau_{исп}}{\tau_{пр}} = \text{idem}$, $\frac{\tau_{см}}{\tau_{пр}} = \text{idem}$, $\frac{\tau_x}{\tau_{пр}} = \text{idem}$.

The elementary stages of the combustion process do not take place sequentially, one after the other, but with some overlap: vaporization and mixing, mixing and chemical reaction and so on take place simultaneously to some degree. Consequently, the overall combustion time is not equal to the sum of the time for the individual process stages, but is always shorter:

$$\frac{\tau_{см}}{\tau_{пр}} + \frac{\tau_{исп}}{\tau_{пр}} + \frac{\tau_x}{\tau_{пр}} > \frac{\tau_{гор}}{\tau_{пр}}. \qquad (7.10)$$

In this case simple summation of the individual stages leads to a large error in determining the combustion time. The slowest of these stages will limit the combustion process and determine the fuel burnup rate. Depending on the construction of the combustion chamber and its elements, the type of fuel and the fineness of its atomization, the chamber operating parameters and loading, the time for one of the stages may exceed considerably the time for the others and, consequently, the faster stages will be completed during the time that the slower stage takes place, i.e., the following relations must be valid:

$$\left.\begin{aligned}
&\text{if } \tau_{хим} > \tau_{см} + \tau_{исп}, \text{ then } \tau_{гор} = \tau_{хим} \text{ and } \eta_{сг} = f_1\left(\frac{\tau_x}{\tau_{пр}}\right);\\
&\text{if } \tau_{см} > \tau_{хим} + \tau_{исп}, \text{ then } \tau_{гор} = \tau_{см} \text{ and } \eta_{сг} = f_2\left(\frac{\tau_{хим}}{\tau_{пр}}\right);\\
&\text{if } \tau_{исп} > \tau_{хим} + \tau_{см}, \text{ then } \tau_{гор} = \tau_{исп} \text{ and } \eta_{сг} = f_3\left(\frac{\tau_{исп}}{\tau_{пр}}\right).
\end{aligned}\right\} \qquad (7.11)$$

Consequently, in each individual case the combustion completeness will be determined by the relative time for the slowest stage.

To determine the limiting stage from experimental data we must investigate the influence of the operating parameters (pressure and temperature) on the time for the individual stages for a constant flowtime.

The chemical reaction time, according to the Arrhenius law, is proportional to:

$$\tau_{хим} \sim \frac{e^{\frac{E}{RT}}}{p^{a+\beta} c_T^a c_\alpha^\beta}. \qquad (7.12)$$

This relation shows that the chemical reaction time decreases exponentially with temperature increase, and decreases with pressure increase to a power equal to the over-all reaction order.

The mixing time is proportional to [31, 32, 33]:

$$\tau_{см} \sim \frac{d^2}{D}, \qquad (7.13)$$

where d is the characteristic dimension;

D is the diffusion coefficient.

It is known that mixing in combustion chambers takes place as a result of turbulent and molecular diffusion, where both these processes proceed in parallel and, consequently, the over-all mixing time is [33]:

$$\tau_{см} = \frac{1}{\frac{1}{\tau_{см_T}} + \frac{1}{\tau_{см_м}}} \sim \frac{d^2}{D_T + D_м}, \qquad (7.14)$$

where $D_T = A w D$ and $D_м = D_0 \left(\frac{T}{T_0}\right)^2 \frac{1}{P}$ are, respectively, the turbulent and molecular diffusion coefficients. For combustion chamber operating conditions [33]:

$$D_T = (20-200) \times 10^{-3} \text{ m}^2/\text{s};$$
$$D_м = (0{,}05-0{,}25) \times 10^{-3} \text{ m}^2/\text{s},$$

and their ratio $\frac{D_T}{D_м} \approx (4-8) \cdot 10^2$. Since D_t is many times larger than D_m, the molecular diffusion coefficient may be neglected. Consequently, we can consider that the mixing in combustion chambers is determined only by turbulent diffusion:

$$\tau_{см} \sim \frac{d^2}{D_T}. \qquad (7.15)$$

According to the Sreznevskiy law, the droplet vaporization time equals:

$$\tau_{исп} = \frac{\delta_к^2}{k}, \qquad (7.16)$$

where δ_k is the maximal droplet diameter, which may be determined using the technique presented in Chapter 4; k is the vaporization constant, which depends both on the fuel physical and chemical properties and on the heat- and mass-transfer conditions at the droplet surface.

Experimental and theoretical data obtained by various authors [34, 35, 36, 37] show that the vaporization constant decreases with increase of pressure and increases with increase of temperature:

$$k \sim \frac{T_\phi^n}{p^s}, \qquad (7.17)$$

where the exponents from various data are:

$$n \approx 2;\ s = 0{,}1 - 0{,}4.$$

The flowtime, which characterizes the combustion chamber loading, is proportional to the combustion chamber length and inversely proportional to the velocity; in the general form it is written as:

$$\tau_{sp} = \int_0^{L_k} \frac{dx}{w_{xcp}}, \qquad (7.18)$$

where

$$w_{xcp} = \frac{1}{R}\int_0^R w_x dr..$$

Usually the nature of the velocity variation along the flametube length and radius is not known in the actual combustion chambers, therefore for the practical determination of the flowtime we can utilize the average relationship for the individual segments of the flametube:

$$\Delta\tau_{sp} = \frac{\Delta L_{pl}}{w_{xcp}} = \frac{\gamma_r D_{p.t}^3 \Delta l}{G_r} \cdot 0{,}785 \text{ s}, \qquad (7.19)$$

where w_{xsr} is the average gas flow velocity over a given segment;

ΔL_{pl} is the length of the given segment, m;

$D_{p.t}$ is the flametube diameter, m;

G_g is the gas flowrate in the segment, kg/s;

Δl is the relative segment length;

γ_g is the gas specific weight, kg/m^3.

The total flowtime up to a given section equals the sum of the flowtimes for each segment:

$$\tau_{sp_n} = \sum_1^n \Delta\tau_{sp} \text{ s}. \qquad (7.20)$$

BURNING LIQUID FUEL

The process of liquid fuel combustion has been studied in experimental and industrial combustion chambers which differ in construction and operating parameters.

The effect of the operating parameters on the magnitude of the

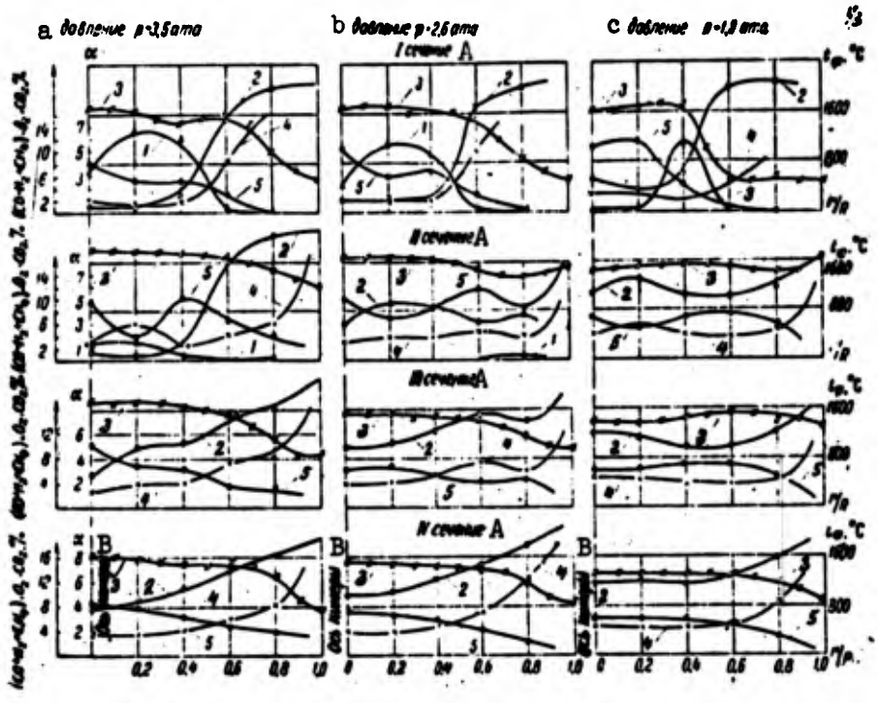

Fig. 48. Distribution of flame temperature, excess air and gas composition across combustion chamber sections: a, b, c) p = 3.5, 2.6 and 1.9 atm abs, respectively; $1-CO+H_2+CH_4$; $2-O_2$; $3-t_\phi$; $4-\alpha$; $5-CO_2$; a) Pressure p = = 3.5 atm abs; b) pressure p = 2.6 atm abs; c) pressure p = 1.9 atm abs, A) Section; B) chamber centerline.

chemical and mechanical incomplete combustion along the chamber length has been studied in several experimental installations with flametubes of diameter 270, 400, 540 and 640 mm [1, 9, 10, 15, 27, 28].

Figure 48 shows curves of the flame temperature, gas composition and excess air distribution at four sections of the chamber of diameter 400 mm, developed for GT-100-750 with pressures of 1.9, 2.6 and 3.5 atm abs and for the same t_a=280°C, $\alpha_{общ}$=5.9; $U_F=6\cdot10^6$ kcal/m$^2\cdot$h atm abs.

In the central zone, characterized by relatively uniform temperature profile, the combustion is not intense because of the oxygen deficiency and the fuel decomposition is primarily pyrogenetic. Combustion does not develop in the peripheral zone because of the fuel deficiency and low temperature. The existence of a radial gradient of the concentrations and axial velocity, and also the

presence of a radial flow causes diffusive and convective mass transfer between the zones and at the location where a nearly stoichiometric fuel-air mixture ratio is reached the chemical reaction of fuel oxidation takes place, and the combustion zone has considerable width $\left(\frac{r}{R}=0{,}5-0{,}7\right)$ because of the presence of large-scale turbulence. The combustion zone takes on an increasingly diffused nature in the direction of gas motion and finally the zone merges in the center if the degree of forcing is sufficiently high. The curves of the temperature, excess air and O_2 and CO_2 concentrations are practically the same for various pressures, however the width of the maximal CO, H_2, CH_4 concentration zone in the chamber head sections increases with increasing pressure (for P = o.9 atm abs r/R = 0.3-0.5, for P = 2.6 atm abs r/R = 0.2-0.5 and for P = 3.5 atm abs, r/R = 0.1-0.5). Increase of the maximal concentration zone width leads to an increase of the flame front thickness, while increase of the average liquid and gasified fuel concentration leads to an increase of the chemical and mechanical incomplete combustion in the sections, with this increase being particularly marked in the head region of the chamber and slight in the tail sections [27], which is illustrated in Fig. 49. We see from Fig. 49 that increase of the pressure from 1.9 to 3.5 atm abs leads to an increase of the chemical and mechanical incomplete combustion nearly by a factor of two over the relative flametube length $L_{cr}/D_{n.т}$=0,3–0,4. This situation is illustrated even more vividly in the same figure in the form of the curve $\eta_{cr}=f(L_{cr}/D_{n.т})$. For example, at the section $L_{cr}/D_{n.т}$=0,4 the combustion completeness for a chamber pressure P = 1.9 atm abs equals 80%, with increase of the pressure to 3.5 atm abs the latter decreases to 55%. Where the fuel has basically vaporized and gasified, the effect of the pressure is reduced considerably, which is observed in the tail regions of the chamber. The curves (see Fig. 49) are approximated by the equation

$$\eta_{cr}=\frac{A}{p^{s}},$$

where s = 0.4 at section 1, s = 0.2 at section 2 and s = 0.02 at section 3.

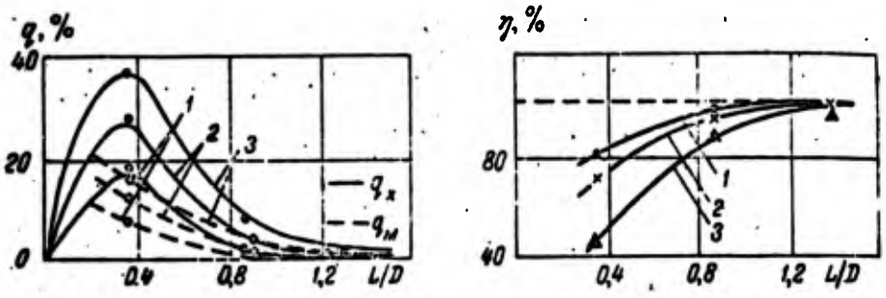

Fig. 49. Variation of chemical and mechanical incomplete combustion along chamber length for various pressures but with the same degree of forcing, U_F=(5,8–6)·10⁶ kcal/m²·h·atm abs; 1, 2, 3) p = 1.94, 2.54, 3.44 atm abs, respectively.

Whether or not vaporization of the atomized fuel is the limiting factor in the over-all process of fuel conversion into the working

gas obviously depends on the type of fuel and droplet dimensions. In our experiments [1, 27, 28] and in several other studies [31, 35, 36, 37] it is noted that if the droplet dimension does not exceed 50-100 microns, the droplets are evaporated in the preheating zone and a mixture of fuel vapors and air enters the reaction zone. Obviously in this case droplet evaporation will occur practically instantaneously, and the process will develop just as in the diffusion flame when burning gas. When the fuel droplet dimensions exceed ~150 microns, we will be concerned with the evaporation and burning of individual droplets. This is confirmed by the experimental data presented above, which show that with increase of the medium pressure the fuel burnup completeness decreases somewhat, while if the combustion took place in the kinetic region the combustion completeness should increase.

Thus, under the conditions of burning liquid fuel (solar oil, distillate oil, fuel oil) under pressure, when the average droplet dimension exceeds ~150 microns, and the maximal dimension of droplets constituting 5-10% by weight equals 350-600 microns, taking into account the fact that fuel vaporization is proportional to the square of the droplet diameter and the evaporation rate decreases with pressure increase, we can assume that from the entire sum of sequential liquid fuel combustion stages the combustion completeness is limited by evaporation and burnup of individual droplets. Experimental data obtained on various combustion chambers make it possible to find the relationship between combustion completeness and the parameter which characterizes the relative vaporization time. The relative vaporization time with account for (7.16) and (7.19) may be written as:

$$\frac{\tau_{исп}}{\tau_{пр}} = \frac{\delta_к^2 w_{ср}}{k L_{п.т}} \sim \frac{\delta_к^{2,25} w_{ср}}{T_ф^{3} L_{п.т}}. \qquad (7.21)$$

The average gas velocity is

$$w_{ср} \sim \frac{G_п T_ф}{P D_{п.т}^2}. \qquad (7.22)$$

Considering that $L_{п.т} = l_x D_{п.т}$, we finally obtain:

$$\frac{\tau_{исп}}{\tau_{пр}} \sim \frac{\delta_к^2 G_п}{P^m T_ф l_x D_{п.т}^3} = \Pi_{исп}, \qquad (7.23)$$

where $m = 1 - s$ and in accordance with the experimental data,

$$m = 0.6 \text{ for } \frac{L_{or}}{D_{п.т}} = 0{,}37;$$

$$m = 0{,}8 \quad , \quad \frac{L_{or}}{D_{п.т}} = 0{,}87;$$

$$m = 0{,}98 \quad , \quad \frac{L_{or}}{D_{п.т}} = 1{,}37.$$

δ_k is the maximal diameter of a droplet atomized by the fuel spray nozzle, m;

G_n is the gas flowrate up to the given section, kg/h;

l_x is the relative flame tube length up to the given section;

P is the chamber pressure, atm abs;

T_f is the flame temperature, °K.

Consequently, for combustion chambers operating on liquid fuel, when the modeling conditions are satisfied and when droplet vaporization is the limiting stage, the combustion completeness is a function of Π_{isp}:

$$\eta_{cr} = f(\Pi_{исп}). \qquad (7.24)$$

Strictly speaking, Relation (7.24) is valid for geometrically similar combustion chambers; nevertheless experience shows that a single curve can correlate combustion chambers which are similar in construction and operating regimes.

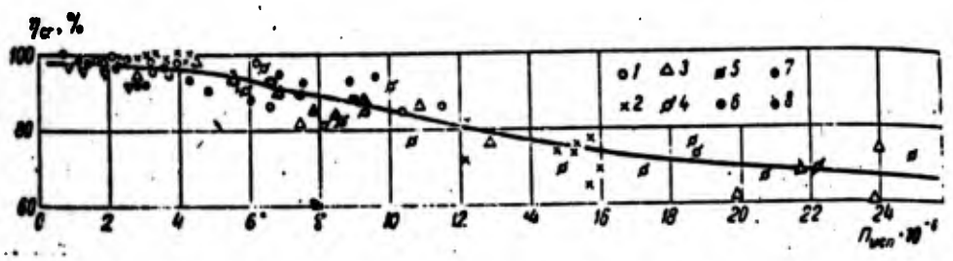

Fig. 50. Combustion completeness η_{s_t} versus vaporization parameter $\Pi_{исп}$ ($\alpha_1 = 1{,}2-1{,}5$, $t_в = 200-280$° C, $t_{к.с} = 700-750$° C, fuel is solar oil, distillate oil, M-20 fuel oil): 1) ГТ-100-750, $D_{в.т} = 640$ mm; 2) ГТ-100-750, $D_{в.т} = 400$ mm; 3) block of combustion chambers ГТ-100-750, $D_{в.т} = 270$ mm; 4) ГТУ-4-750 КТЗ, $D_{в.т} = 270$ mm; 5) ГТ-1,5-700 НЗЛ, $D_{в.т} = 306$ mm; 6, 7, 8) experimental chambers, $D_{p.t}$ = 400, 360, 540 mm, respectively.

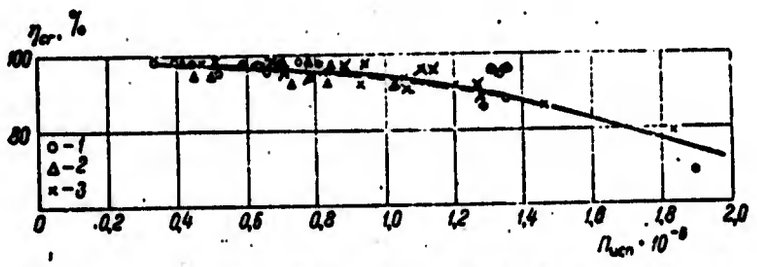

Fig. 51. Relation $\eta_{cr} = f(\Pi_{исп})$ for large-scale models of multiregister combustion chambers (type ГТ-25-700): 1, 2, 3) Models No. 1, 2, 3, respectively; $D_{в.т} = 640, 510, 396$. fuel is solar oil.

Figure 50 presents the relations $\eta_{cr} = f(\Pi_{исп})$ for eight experimental and industrial combustion chambers, while Fig. 51 shows the relation for three large-scale models of multiregister combustion chambers [10] (type ГТ-25-700) burning liquid fuel. We see from these curves

that the relations for the combustion completeness η_{sg} are correlated quite satisfactorily by the evaporation parameter Π_{isp} and are approximated by the equation

$$\eta_{cr} = \left(1 - e^{-\frac{B}{\Pi_{исп}}}\right) \times 100\%, \qquad (7.25)$$

where the empirical coefficient B characterizes the chamber construction and its operation. The quantity B has the same value for combustion chambers which are geometrically similar and of comparable construction: $B = 22$ for the chambers of Fig. 50, $B = 2.6$ for the chambers of Fig. 51.

The conditions for approximate similarity of the combustion process of atomized liquid fuel if evaporation is the limiting stage may finally be written:

1) geometrical similarity of the combustion chambers;

2) $\alpha_{общ} = \text{idem}$, $\alpha_1 = \text{idem}$, $t_в = \text{idem}$, $\beta_ф = \text{idem}$ and the same fuel;

3) $\Pi_{исп} = \text{idem}$ or $\frac{\tau_{исп}}{\tau_{пр}} = \text{idem}$.

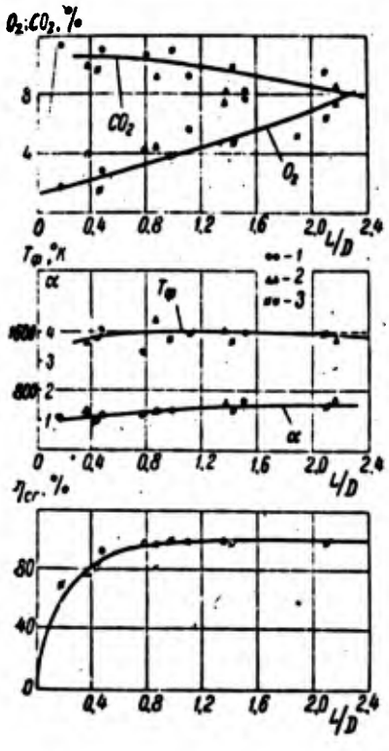

Fig. 52. Variation of oxygen and carbon dioxide concentration, flame temperature, excess air and fuel combustion completeness along flametube length for three combustion chamber models ГТ-100-750 ЛМЗ.

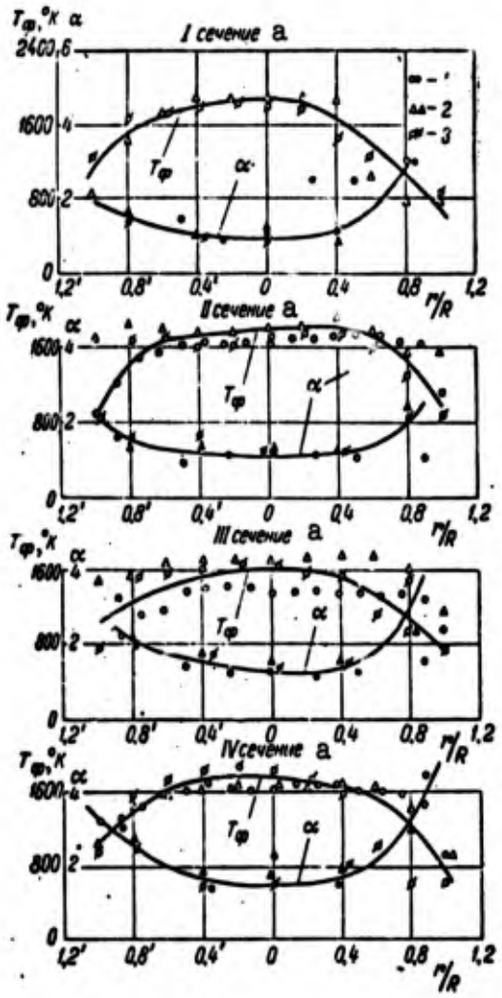

Fig. 53. Variation of flame temperature and excess air along radius of flametube for three combustion chamber models ГТ-100-750 ЛМЗ (fuel is distillate oil). a) Section.

To illustrate the validity of the conditions for hot-flow modeling when burning liquid fuel, Figs. 52 and 53 present curves of the distribution of the O_2 and CO_2 concentrations, excess air, flame temperature along the radius and length of the flametube, and also curves of the burnup for three combustion chamber models ГТ-100-750 when the modeling conditions indicated above are satisfied. The notations for the experimental points in these figures are given in Table 7.1. We see from the curves that the experimental points are grouped with only slight scatter around curves which are common for the three chambers. This confirms the identity of the flame structure and combustion completeness for geometrically similar chambers.

With the aid of the relation $\eta_{cr}=f(\Pi_{исп})$, constructed from the data of model chamber tests on an experimental stand, we can determine the combustion completeness in the full-scale combustion chamber operating in the GTE arrangement. To do this we must determine the

values of the parameter Π_{isp} for full-scale conditions and from the curve $\eta_{cr}=f(\Pi_{isp})$ constructed for the model we determine the combustion completeness.

TABLE 7.1

Обозначение точек a	№ опыта b	$D_{п.т}$	$\alpha_{общ}$	α_1	$t_в$	$t_{ух}$	P	$u_р$	$\Pi_{исп}$
1	30	640	5,53	1,56	276	732	1,82	5,56	3,26
2	17	400	5,97	1,53	275	750	2,62	5,40	3,76
3	11	270	5,35	1,45	302	736	3,54	5,03	2,97

a) Point designation; b) experiment.

Table 7.2 presents the sequence and a numerical example of the conversion of combustion completeness from model to full scale.

The parameter Π_{isp} is approximate and therefore does not take into acccunt the entire complexity of the phenomena of heat and mass transfer during relative motion of the evaporating droplets, therefore for a more complete determination of the relative evaporation time we must take into account the droplet deceleration time. In the following, we present a theoretical derivation of the time for complete droplet evaporation.

When leaving the fuel spray nozzle the droplets travel relative to the air, and if the droplet velocity is greater than the flow velocity the droplet is retarded; if the droplet velocity is greater than the flow velocity the droplet is accelerated. After equalizing the flow and droplet velocities, the latter moves together with the gas stream and droplet evaporation and combustion are described by diffusion theory [38, 39].

During droplet motion relative to the stream (dynamic region) the evaporation and combustion process is described by the equations of motion, heat transfer and mass transfer:

$$\frac{dc}{d\tau}=-\frac{R}{m}; \tag{7.26}$$

$$\frac{dQ}{d\tau}=\alpha F_к(T_ф-T_к); \tag{7.27}$$

$$\frac{dG}{d\tau}=\beta F_к(P_{пк}-P_{п.ф}). \tag{7.28}$$

The quantities appearing in (7.26, 7.27, 7.28) denote:

$R=C_R F_м \frac{v^2\gamma_г}{2g}$ is the droplet resistance;

$m=\frac{\pi\delta_к^3\gamma_т}{6g}$ is the droplet mass;

$F_к = \pi\delta_к^2$ is the droplet surface area;

$\alpha = \frac{Nu_т\lambda}{\delta_к}$ is the heat release coefficient;

$\beta = \frac{Nu_g D_п}{\delta_к R_п T_к}$ is the evaporation coefficient, referred to the difference of the partial pressures.

On the basis of the analogy between heat and mass transfer [35, 38, 40], we can take

$$Nu_т = Nu_g = bRe^{0.5},$$

where $P_{п.к} = e^{-\frac{A}{T_к + C} + B}$ is the partial pressure of the vapor at the droplet surface [31, 40].

$P_{п.ф}$ is the vapor partial pressure in the combustion region (may be taken equal to zero).

After transforming (7.26, 7.27, 7.28), we obtain

$$\frac{dv}{d\tau} = -\frac{3}{4}\cdot\frac{L\gamma_т\nu_п^{0.5}}{4\gamma_т}\left(\frac{v}{\delta_к}\right)^{1.5}; \qquad (7.26a)$$

$$\frac{d\delta_к}{d\tau} = -\frac{2Nu_т\lambda(T_ф - T_к)}{\gamma_т\Delta i\delta_к} = -\frac{2\lambda_п b(T_ф - T_к)}{\gamma_т\Delta i\nu_п^{0.5}}\left(\frac{v}{\delta_к}\right)^{0.5}; \qquad (7.27a)$$

$$\frac{d\delta_к}{d\tau} = -\frac{2Nu_g D_п(P_{п.к} - P_{п.ф})}{\gamma_т\delta_к} = -\frac{2D_п b(P_{п.к} - P_{п.ф})}{\gamma_т\nu_п^{0.5}R_п T_к}\left(\frac{v}{\delta_к}\right)^{0.5}. \qquad (7.28a)$$

From (7.26a) and (7.27a), we find the relation between droplet diameter and velocity

$$\frac{\delta_к}{\delta_0} = \left(\frac{v}{v_0}\right)^A, \qquad (7.29)$$

where δ_0 and v_0 are the initial droplet diameter and relative velocity; $\delta_к$ and v are the instantaneous diameter and velocity.

$$A = \frac{8\lambda b(T_ф - T_к)}{3L\Delta i\gamma_т\nu_п}.$$

Substituting the value of v from (7.29) into (7.28a) and integrating over the limits from 0 to τ and δ_0 to $\delta_к$, we obtain

$$\delta_0^a - \delta_к^a = k_1\tau, \qquad (7.30)$$

where $k_1 = \frac{bD_п(P_{п.к} - P_{п.ф})v_0^{0.5}(3A-1)}{\gamma_т\nu_г^{0.5}\delta_0^{1/2A}AR_п T_к}$ is the dynamic evaporation constant;

$a = 1{,}5 - \frac{1}{2A}$ is the exponent.

TABLE 7.2

a № пп.	b Наименование	c Обозначение	d Размерность	e Формула	f Пример ГТ-100-750		
					$D_{п.т}$=270 g модель	$D_{п.т}$=400 g модель	$D_{п.т}$=100 h натура
1	Давление в камере	P	i $ата$	j Из расчета схемы ГТУ	3,39	2,58	26
2	Максимальный диаметр капли	$\delta_к$	$м$	k Из расчета форсунки	$195 \cdot 10^{-6}$	$373 \cdot 10^{-6}$	$414 \cdot 10^{-6}$
3	Температура воздуха	$T_в$	°K	j Из расчета схемы ГТУ	559	546	550
4	Избыток воздуха в сечении	α_1	—	l Из теплового расчета камеры сгорания	1,7	1,85	1,80
5	Низшая теплотворная способность топлива	$Q_р^н$	m $\frac{ккал}{кг}$	m То же	9801	9701	9801
6	Теоретический расход воздуха	L_0	o $\frac{кг}{кг}$		14,1	14,1	14,1
7	Тепло, внесенное в камеру	$Q_{вн}$	m $\frac{ккал}{кг}$	$Q_р^н + c_{рт} t_т + \alpha_1 L_0 c_{рв} t_в$	11 560	11 420	11 500
8	Температура факела	$T_ф$	°K	p Из уравнения теплового баланса	1865	1793	1793
9	Средний расход газов до сечения	$G_п$	q $кг/ч$	$G_р + G_{щ} + B_т$	5282	8086	43 800
10	Диаметр пламенной трубы	$D_{п.т}$	$м$	r Из теплового расчета камеры сгорания	0,27	0,4	0,4
11	Относительная длина до определяемого сечения	l_x	—	$L_{п.т}/D_{п.т}$	1,42	1,37	1,37
12	Показатель степени при давлении	m	—	s По опытным данным $L/D = 0{,}37$, 0,87 и 1,37 $m = 0{,}6$, 0,8 и 0,98 соответственно	0,97	0,96	0,96
13	Параметр испарения	$Ш_{исп}$	$\frac{т}{кг / ч \cdot ата \cdot м \cdot °K}$	$\frac{\delta_к^2 G_п}{P^m T_ф l_x D_{п.т}^3} \cdot 10^{-}$	2,99	2,88	2,10
14	Полнота сгорания расчетная	$\eta_{сг}^{р}$	%	u По кривой рис. 50	98,4	98,5	98,8
15	Полнота сгорания опытная	$\eta_{сг}^{оп}$	%	v По опытным данным	98,5	99,0	—

a) No.; b) item; c) symbol; d) dimension; e) formula; f) example; g) model; h) full-scale; i) atm abs; j) from analysis of GTE cycle; k) from spray nozzle analysis; l) from thermal analysis of combustion chamber; m) kcal/kg; n) the same; o) kg/kg; p) from heat balance equation; q) kg/h; r) from combustion chamber thermal analysis; s) from experimental data, L/D = 0.37, 0.87 and 1.37, m = 0.6, 0.8 and 0.98, respectively; t) kg/h·atm abs·m·°K; u) from curve of Fig. 50; v) from experimental data. 1) Chamber pressure; 2) maximal droplet diameter; 3) air temperature; 4) excess air at section; 5) fuel lower heating value; 6) theoretical air flowrate; 7) heat introduced into chamber; 8) flame temperature; 9) average gas flowrate up to section; 10) flametube diameter; 11) relative length to section in question; 12) pressure exponent; 13) vaporization parameter; 14) theoretical combustion completeness; 15) experimental combustion completeness.

We obtain the deceleration time from (7.26a) by replacing δ_k by its value from (7.29):

$$\tau_{торм} = -\frac{4\gamma_т \delta_0^{1,5}}{3L\gamma_т v_в^{0,5} v_0^{1,5A}} \int_{v_0}^{v} v^{1,5(A-1)}\, dv. \qquad (7.31)$$

After integrating for v = 0, we obtain

$$\tau_{торм} = \frac{8\gamma_т \delta_0^{1,5}}{3L\gamma_т v_в^{0,5}(3A-1)} v_0^{-0,5}. \qquad (7.32)$$

During the deceleration time the droplet dimension decreases to the value

$$\delta_{кт} = (\delta_0^a - k_1\tau_т)^{1/a}. \qquad (7.33)$$

The axial component of the droplet relative initial velocity is

$$v_0 = c_x - w_x,$$

where $c_x = \frac{\mu}{\varphi}\sqrt{\frac{2g\Delta P}{\gamma_т}}$ is the axial component of the fuel discharge velocity from the spray nozzle;

$w_x = w\cdot\cos\left(\frac{\beta_к}{2} - \alpha_л\right)\cos\frac{\alpha_л}{2}$ is the axial component of the air velocity at the register exit;

$\frac{\mu}{\varphi}$ is the ratio of the spray nozzle discharge coefficient to the effective section coefficient [22];

$\beta_к$, $\alpha_л$ are the cone angles of the flametube and the register vane;

$w = \frac{G_в}{F_{в вых}\gamma_в}$ is the air velocity in the intervane space.

During the deceleration time the droplet velocity equalizes the flow velocity (v = 0), and in this case with some approximation

we can consider that the droplet travels together with the flow, the droplet combustion process is diffusive and symmetric relative to the droplet center [38, 39]. The droplet combustion scheme is then the following: oxygen diffuses from the surrounding medium to the droplet surface, and fuel vapors diffuse from the droplet surface. In the zone of approximately stoichiometric fuel-oxygen mixture ratio, a spherical combustion zone is established and, since the chemical reactions take place practically instantaneously, the thickness of the combustion zone is negligibly small and the fuel vapors and oxygen do not pass through the combustion zone.

The system of equations for heat and mass transfer is then the following.

1. Heat flux from combustion zone to droplet surface

$$Q_1 = 4\pi r^2 \lambda_n \frac{dT}{dr}. \tag{7.34}$$

2. Fuel vapor mass flux from droplet to combustion zone

$$G_n = -4\pi r^2 \frac{D_n P}{R_n T} \cdot \frac{dc}{dr}. \tag{7.35}$$

3. Heat flux from combustion zone to surrounding space

$$Q_2 = -4\pi r^2 \lambda_к \frac{dT}{dr}. \tag{7.36}$$

4. Oxygen mass flux from surrounding medium to combustion zone

$$G_к = 4\pi r^2 \frac{D_к P}{R_к T} \cdot \frac{dc}{dr}. \tag{7.37}$$

Additional relations must be introduced to solve this system of equations.

The heat expended on evaporation is

$$Q_1 = G_n \Delta l = G_n (q_{исп} + c_{рп} \Delta t). \tag{7.38}$$

The heat released during fuel combustion is

$$Q_1 + Q_2 = G_n q_{гор}. \tag{7.39}$$

The stoichiometric relation

$$G_к = 0{,}23 L_0 G_n = L_{ок} G_n. \tag{7.40}$$

In the above equations the diffusion and heat conduction coefficients are as follows [31, 35, 40]:

$$D = D_0 \left(\frac{T_ф}{T_0}\right)^2 \frac{P_0}{P}; \quad \lambda_n = \lambda_{оп} \left(\frac{T_ф}{T_0}\right); \quad \lambda_к = \lambda_{ок} \frac{T_ф}{T_0}. \tag{7.41}$$

Solving the system of equations presented above and considering that the vaporization rate equals

$$G_n = -\frac{dP}{d\tau} = -\frac{\pi\delta_k^2}{2}\gamma_r \cdot \frac{d\delta_k}{d\tau}, \qquad (7.42)$$

we obtain the time dependence of the droplet diameter for static vaporization

$$\delta_{k.r}^2 - \delta_{k.np}^2 = k_2\tau_{cr}, \qquad (7.43)$$

where $\delta_{k.t}$ is the droplet diameter at the end of the deceleration time;

k_2 is the static vaporization constant:

$$k_2 = \frac{4}{\gamma_k}\left\{\frac{\lambda_{ok}T_\phi^2}{\Delta i T_0}\left[(M+1)^2 - \left(\frac{T_k}{T_\phi}\right)^2\right] + \frac{\lambda_{ok}T_\phi^2}{Q_p^n T_0}\left[(M+1)^2 - 1\right]\right\}, \qquad (7.44)$$

where

$$M = \frac{D_{ok}P_0 Q_p^n c_k}{L_{ok}\lambda_{ok}R_k T_0 T_\phi};$$

$c_k = O_2\frac{\gamma_{O_2}}{\gamma_r}b\frac{1}{100}$ kg/kg is the relative oxygen weight concentration.

$$c_k = \frac{0{,}232L_0}{\alpha_1 L_0 + 1}(\alpha_1 - \eta_{cr})\frac{\text{kg}}{\text{kg}}. \qquad (7.45)$$

The total vaporization time in the static region is

$$\tau_{cr} = \frac{\delta_{k.r}^2}{k_2}. \qquad (7.46)$$

The total vaporization time equals the sum of the deceleration time and the evaporation time in the region of "static" particle motion:

$$\tau_{исп} = \tau_{торм} + \tau_{cr}. \qquad (7.47)$$

To verify the validity of the relations presented above a calculation was made of the deceleration time and the static vaporization time on the basis of experimental data for various combustion chambers. The resulting values of the relative total vaporization time (τ_{isp}/τ_{pr}) were correlated by the relation

$$\eta_{cr} = f\left(\frac{\tau_{исп}}{\tau_{пр}}\right). \qquad (7.48)$$

Figure 54 presents this relation for three ГТ-100-750 combustion chamber models with flametube diameters 640, 400 and 270 mm; ГТУ-4 КТЗ with $D_{p.t}$ = 270 mm; ГТ-700 НЗЛ with $D_{p.t}$ = 505 mm and an experimental fuel oil chamber with $D_{p.t}$ = 400 mm.

The experimental curve is approximated by the relation

$$\eta_{cr} = \left(1 - e^{-B\frac{\tau_{пр}}{\tau_{исп}}}\right) \times 100\%, \text{ where } B = 6{,}1.$$

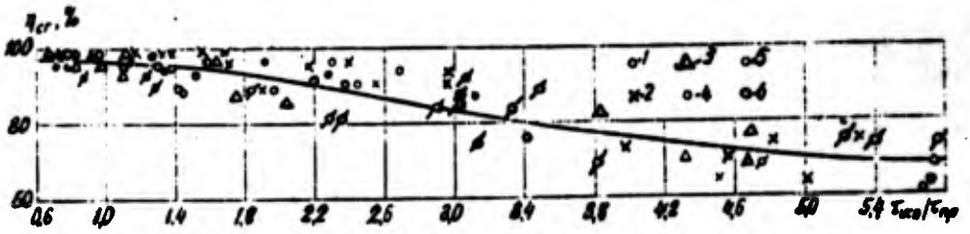

Fig. 54. Relation $\eta_{cr} = f\left(\frac{\tau_{исп}}{\tau_{пр}}\right)$ for $\alpha_1 = 1{,}2-1{,}5$; $t_в = 200-280°C$; $t_{к.с} = 700-750°C$: 1, 2, 3) ГТ-100-750, $D_{п.т} = 610$, 400, 200 mm, respectively; 4) ГТУ-4 КТЗ, $D_{п.т} = 290$ mm; 5) ГТ-700 НЗЛ, $D_{п.т} = 505$ mm; 6) experimental chamber, $D_{п.т} = 400$ mm.

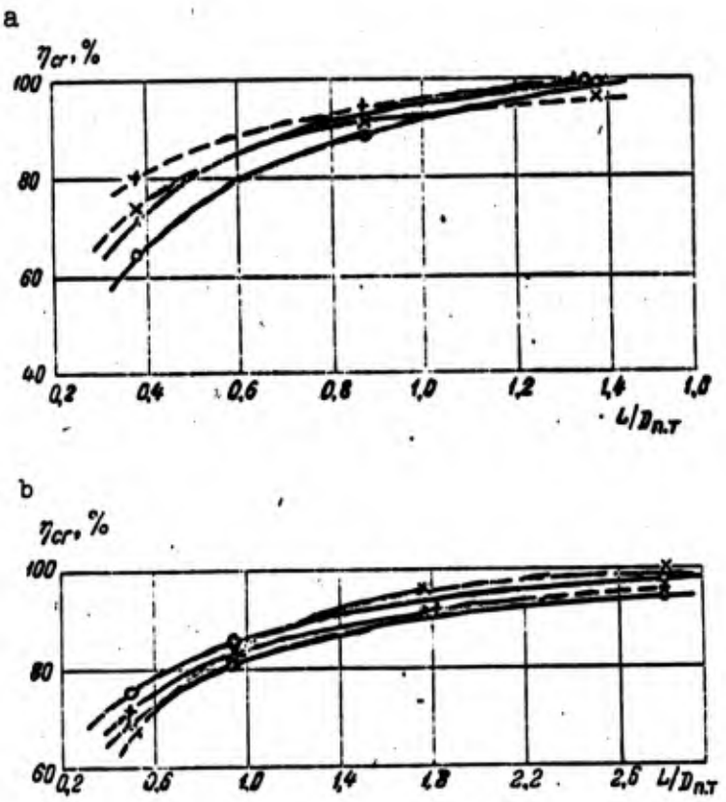

Fig. 55. Comparison of theoretical and experimental burnup curves: a) Chamber ГТ-100-750 ЛМЗ, $D_{п.т} = 400$ mm; b) chamber ГТУ-4-750 КТЗ, $D_{п.т} = 270$ mm; -----) Theoretical; ———) experimental.

Table 7.3 presents the scheme and an example of the calculation of droplet evaporation time and combustion completeness for any flametube length. On the basis of this calculation we can plot the burnup curves for an analogous chamber for various operating parameters.

Figure 55 shows as an example for several experiments the results of a comparison of the burnup curves obtained in experiments and those calculated using the scheme described above for complete droplet burnup.

TABLE 7.3

1 Наименование величин	2 Обозначение	3 Размерность	4 Расчетная формула	5 Примечание	6 Пример расчета	
					ГТ-100-750	ГТУ-4-750
7 Исходные данные						
8 Давление в камере (абс.)	P	9 кг/см²	10 Из расчета схемы ГТУ		2,56	4,8
11 Температура факела	$T_ф$	°К	12 Из уравнения теплового баланса		1688	1737
13 Перепад давления на форсунке	ΔP	14 кг/см²	15 Из расчета форсунки		53,9	32,2
16 Максимальный диаметр капли	$\delta_м$	м	17 Из расчета форсунки или по формуле $k\sqrt{\frac{M}{\Delta P}}$		$320\cdot10^{-6}$	$287\cdot10^{-6}$
18 Скорость воздуха на выходе из регистра	$w_р$	19 м/сек	20 Гидравлический расчет		73,6	47,6
21 Удельный вес топлива	$\gamma_т$	22 кг/м³	23 Из теплового расчета		$0,877\cdot10^3$	$0,827\cdot10^3$
24 Удельный вес газов	$\gamma_г$	22 кг/м³	$\frac{P}{R_г T_ф}$		0,548	0,997
25 Концентрация кислорода в факеле	$C_к$	26 кг/кг	$\frac{0,232L_0}{\alpha L_0+1}(\alpha-\gamma_{сг})$		0,0950	0,0317
27 Определение физических констант						
28 Коэффициент кинематической вязкости паров топлива	$\nu_п$	29 м²/сек	$0,72\left(\frac{T_ф}{T_0}\right)^{1,8}\cdot\frac{1}{P}\cdot10^{-6}$		$7,4\cdot10^{-6}$	$4,16\cdot10^{-6}$
30 Коэффициент молекулярной диффузии паров	$D_п$		$4,6\left(\frac{T_ф}{T_0}\right)^{2}\cdot\frac{1}{P}\cdot10^{-6}$		$68,8\cdot10^{-6}$	$38,6\cdot10^{-6}$

TABLE 7.3 CONTINUED

31 Коэффициент теплопроводности паров топлива	$\lambda_п$	32 $\frac{ккал}{м \cdot сек \cdot град}$	$0{,}29\left(\frac{T_ф}{T_0}\right)^2 \cdot 10^{-5}$			$11{,}1 \cdot 10^{-5}$	$11{,}72 \cdot 10^{-5}$
33 Температура кипения топлива	$T_к$	°К	$T_{к0}P^{0,1}$		$T_{к0}=413$, 34 соляр $T_{к0}=483$, мазут 34	530	483
35 Давление насыщенного пара		36 кг/см²	$e^{\frac{A}{T_к c}+B}$		$\frac{A}{3300}\cdot\frac{B}{9{,}40}\cdot\frac{C}{67}$, 34 соляр $3720\times\times 9{,}42\cdot 91$, дистилят	2,31	4,35
38 Теплоемкость паров топлива	$c_{pп}$	39 $\frac{ккал}{кг \cdot град}$	40 Из таблиц по $T_к$		37	0,51	0,55
41 Теплота испарения	$q_п$	42 $\frac{ккал}{кг}$	$\frac{1}{T_т}(84{,}6-0{,}09T_к)$			42,9	49,4
43 Теплосодержание паров топлива	Δi	42 $\frac{ккал}{кг}$	$q_п + c_{pп}(T_в - T_{топл})$		44 Температура воспламенения $T_в = 841$ °К	296	325
45 **Испарение на динамическом участке**							
46 Коэффициент	A	—	$0{,}115\frac{\lambda_п (T_{ср}-T_к)}{\Delta i \nu_п T_т}$			12,3	12,54
47 Показатель степени	a	—	$1{,}5-\frac{1}{2A}$			1,459	1,46
48 Абсолютная скорость капли (по оси камеры)	c_x	49 м/сек	$\frac{\mu}{\varphi}\sqrt{2g\frac{\Delta P}{T_т}}$	50 A — геометрическая характеристика форсунки	$\frac{\mu}{\varphi}=0{,}563$ $\mu = f(A)$ и $\varphi = f(A)$ 49	62,0	49,2

TABLE 7.3 CONTINUED

1 Наименование величин	2 Обозначение	3 Размерность	4 Расчетная формула	5 Примечание	6 Пример расчета ГТ-100-750	6 Пример расчета ГТУ-4-750
5 1 Абсолютная скорость воздуха (по оси камеры)	w_x	5 2 *м/сек*	$w_p \cos\left(\frac{\beta_к}{2} - \beta_л\right) \cos\frac{\beta_к}{2}$	5 3 $\beta_к$ — угол раскрытия конуса 5 4 $\beta_л$ — угол наклона лопатки	52,0 10,0	33,7 15,5
5 5 Относительная скорость капли	v_{x0}	5 2 *м/сек*	$c_x - w_x$			
5 6 Константа динамического испарения	k_1	5 7 $\frac{м \cdot град}{сек}$	$\frac{1{,}12 D_п P_{в.к} (v_{x0})^{0{,}5} a}{\gamma_т \nu_п^{0{,}5} \delta_м^{1{,}2A}}$		540·10⁻⁶	888·10⁻⁶
5 8 Время торможения капли	$\tau_{торм}$	5 9 *сек*	$\frac{0{,}205 \gamma_т \delta_м^{1{,}5}}{\gamma_т \nu_п^{1{,}5} (v_{x0})^{0{,}5} (3A - 1)}$		6,0·10⁻³	2,98·10⁻³
6 0 Диаметр капли за время торможения	$\delta_{к.т}$	*м*	$(\delta_м^a - k_1 \tau_т)^{1/a}$		224·10⁻⁶	209·10⁻⁶
6 1 Константа статического испарения	k_2	6 2 $\frac{м^2}{сек}$	$\frac{4}{\gamma_т}\left\{2{,}59 \cdot 10^{-11} \frac{T_ф^2}{\Delta l}\left[(M+1)^2 - \left(\frac{T_к}{T_ф}\right)^2\right] + 2{,}19 \cdot 10^{-8}\left[(M+1)^2 - 1\right]\right\}$	$M = 1{,}19 \frac{c_к Q_р^н}{T_ф}$	3,31·10⁻⁶	3,66·10⁻⁶
6 3 Время статического испарения	$\tau_{исп}^{ст}$	6 4 *сек*	$\frac{\delta_{к.т}^2}{k_2}$		15,15·10⁻³	11,9·10⁻³
6 5 Время полного испарения	$\tau_{исп}$	6 4 *сек*	$\tau_{торм} + \tau_{исп}^{ст}$		21,15·10⁻³	14,9·10⁻³
6 6 Определение времени пребывания						
6 7 Длина участка пламенной трубы до сечения	Δl	*м*	6 8 Принимается	6 9 I сечение II . III . IV .	0,148 0,200 0,200 0,320	0,139 0,106 0,236 0,279

TABLE 7.3 CONTINUED

70 Средняя скорость газов на участке	$w_{ср}$	71 м/сек	$\frac{G_n}{F_n \gamma_г}$	69	I сечение	31,5	50,6
					II .	56,0	60,7
					III .	66,7	66,4
					IV .	67,3	66,4
72 Время пребывания до сечения	$\tau_{пр}$	73 сек·10^{-3}	$\sum_1^n \frac{\Delta L_n}{w_{ср\,n}}$; n — число участков	74	I .	4,7	2,75
					II .	8,27	4,49
					III .	11,27	8,05
					IV .	16,02	12,25
75 Отношение времени испарения ко времени пребывания	$\frac{\tau_{исп}}{\tau_{пр}}$		$\frac{\tau_{исп}}{\tau_{пр}}$		I .	4,51	5,42
					II .	2,56	3,32
					III .	1,88	1,85
					IV .	1,32	1,22
76 Полнота сгорания до данного сечения (расчетная)	$\eta_{сг}^{р}$	%	77 По кривой (рис. 54) или по формуле: $\left(1 - e^{-B\left\|\frac{\tau_{исп}}{\tau_{пр}}\right\|}\right) \times 100$, $B = 6{,}1$		I .	74,1	82,6
					II .	90,8	96,0
					III .	96,1	98,9
					IV .	98,0	99,0
78 Полнота сгорания до данного сечения (опытная)	$\eta_{сг}^{оп}$	%	79 Из опыта		I .	64,0	76,1
					II .	88,0	84,9
					III .	98,0	93,0
					IV .	100	99,6

1) Item; 2) symbol; 3) dimension; 4) calculation formula; 5) remarks; 6) calculation example; 7) basic data; 8) chamber pressure (abs); 9) kg/cm^2; 10) from analysis of the GTE cycle; 11) flame temperature; 12) from heat balance equation; 13) pressure drop across spray nozzle; 14) kg/cm^2; 15) from spray nozzle analysis; 16) maximal droplet diameter; 17) from spray nozzle analysis or from the formula; 18) air velocity at register exit; 19) m/s; 20) hydraulic analysis; 21) fuel specific weight; 22) kg/m^3; 23) from thermal analysis; 24) gas specific weight; 25) oxygen concentration in flame; 26) kg/kg; 27) determination of physical constants; 28) fuel vapor kinematic viscosity; 29) m^2/s; 30) vapor molecular diffusion coefficient; 31) fuel vapor heat conductivity; 32) kcal/m·s·deg; 33) fuel boiling temperature; 34) solar oil; 34') fuel oil; 35) saturated vapor pressure; 36) kg/cm^2; 37) distillate oil; 38) fuel vapor specific heat; 39) kcal/kg·deg; 40) from tables for T_k; 41) heat of vaporization; 42) kcal/kg; 43) fuel vapor enthalpy; 44) ignition temperature; 45) vaporization in dynamic region; 46) coefficient; 47) exponent; 48) droplet absolute velocity (along chamber centerline); 49) m/s; 49') and;50) A is the geometrical characteristic of the spray nozzle; 51) air absolute velocity (along chamber centerline); 52) m/s; 53) β_k is the cone aperture angle; 54) β_1 is the vane inclination angle; 55) relative droplet velocity; 56) dynamic vaporization constant; 57) m·deg/s; 58) droplet deceleration time; 59) s; 60) droplet diameter after deceleration time; 61) static vaporization constant; 62) m^2/s; 63) static vaporization time; 64) s; 65) total vaporization time; 66) determination of flow time; 67) length of flametube segment up to section; 68) assumed; 69) section; 70) average gas velocity over segment; 71) m/s; 72) flow time up to section; 73) s; 74) number of segments; 75) ratio of vaporization time to flowtime; 76) combustion completeness up to given section (theoretical); 77) from curve (Fig. 54) or from formula; 78) combustion completeness up to given section (experimental); 79) from experiment.

There is considerable discrepancy between the theoretical and experimental curves in the head region of the chamber, where considerable concentration nonuniformity is observed and it is difficult to make an exact determination of the burnup completeness. Nevertheless, the general agreement of the curves is quite satisfactory, the discrepancy between the experimental and theoretical points for all the experimental data processed does not exceed 20-25% in the head region and 5-10% in the chamber tail regions.

BURNING GASEOUS FUEL

The process of gaseous fuel combustion takes place in two stages: mixing and chemical reactions. Experimental data and direct observation of the flame show that for separate fuel and air input the gaseous fuel combustion process in combustion chambers usually takes place in the diffusion region, which is indicated by the bright-yellow flame coloring and the weak dependence of the flame length on the loading. High pressure and high flame temperature lead to the situation where the chemical reaction rates are excessively high and the combustion process is limited by turbulent mixing of the gas with the air. Only in combustion chambers with burners providing partial

premixing (for example, burners with hollow vanes of the type ГТ-50-800 ХТЗ im. S.M. Kirov) under suitable conditions will combustion take place in the kinetic region, since the mixing of the gas with the air in burners of this type takes place more intensely than in diffusion burners. For all types of burners transition of the process into the kinetic region can occur for partial chamber loading, when the flame temperature decreases sharply because of the excess air increase.

Separate fuel and air input, most widely used in burners of the diffusion type, has definite advantages in comparison with fuel input in burners with premixing. Stable burning of the fuel which is not completely mixed with the air takes place over considerably wider limits with respect to excess air without the occurrence of flameout and pulsation. Gas input into the combustion zone through a large number of holes in the center of the burner creates individual fuel "islands," which burn from the surface, creating a highly-developed and varied flame front.

The presence of this sort of igniting centers increases the over-all combustion stability. This combustion process has been termed "microdiffusion" by Frank-Kamenetskiy [35, 38].

Observations of the gaseous fuel combustion process in combustion chambers show the existence of a continuous luminous flame which is symmetrical about the chamber centerline. A blue flame can be observed only in the peripheral region. The distribution of the flame temperatures, excess air and gas composition along the chamber radius has the same nature as for the burning of liquid fuel.

The central portion of the flame in the head sections is occupied by a reverse flow zone, indicated by a high temperature which is constant along the radius and low excess air. The oxygen concentration in this region is minimal, while the carbon dioxide concentration is maximal. The flame is located around the reverse flow zone, and the combustion front has considerable thickness along the radius. Toward the periphery of the chamber the temperature and CO_2 concentration decrease, while the excess air and oxygen concentration increase, which is caused by swirling of the air flow by the register and entrainment of air from the cooling slots. Experimental data and direct observations indicate that the length of the gaseous flame is usually no less, and sometimes exceeds the length of the liquid fuel flame for the same burner construction and similar operating parameters, which is seen from the burnup curves for liquid and gaseous fuel shown in Fig. 27. The complexity of the entire combustion process, associated primarily with breakdown of the combustion volume into a large number of diffusion microzones, in which the burnup proceeds from the surface of individual "moles," makes it difficult to obtain an analytic relationship for determining the combustion completeness, therefore it is more convenient to correlate the experimental data in dimensionless form.

Considering that for the combustion of gaseous fuel the limiting stage is the mixing, the combustion completeness is expressed in the form of a function of the relative mixing time:

$$\tau_{kr} = f\left(\frac{\tau_{sm}}{\tau_{pr}}\right). \qquad (7.49)$$

As indicated previously, the turbulent mixing time, which determines the entire mixing process, is

$$\tau_{sm_T} \sim \frac{d^2}{D_T}, \qquad (7.50)$$

where $D_T A w_{gor} D_r$ is the turbulent diffusion coefficient;

w_{gor} is the characteristic velocity;

D_r is the register diameter;

A is a factor;

d is the characteristic dimension of the gas channels.

The average value of the gas flow time up to the given section is

$$\tau_{pr} \sim \frac{\gamma_r}{G_n} D_{n.t}^3 l_x \text{ s}, \qquad (7.19a)$$

where G_n is the average gas flowrate up to the given section, kg/s;

γ_g is the average gas specific weight up to the given section, kg/m^3;

$l_x = \frac{L}{D_{n.t}}$ is the relative distance to the given section.

Substituting in place of τ_{sm} and τ_{pr} their values, we obtain the mixing parameter:

$$\Pi_{sm} = \frac{d^2 G_n}{w_{gor} D_r \gamma_r D_{n.t}^3 l_x}. \qquad (7.51)$$

In correlating experimental data on burners of different constructions, we take as the characteristic velocity the stoichiometric velocity of the air and gas flows at the burner exit:

$$w_{gor} = \frac{G_r w_r + L_0 B_T w_r}{G_r + L_0 B_T} = \frac{\alpha_1 w_r + w_r}{\alpha_1 + 1} \text{ m/s}. \qquad (7.52)$$

As the characteristic dimension of the gas channels for correlating the experimental data we have used:

a) for burners with slot-type gas distribution (type ГТН-9-750 and ГТ-25-700 ЛМЗ) $d = \delta_ш$;

b) for burners with "hole-type" gas distribution (type ГТ-100-750 ЛМЗ and ГТУ-6-750 СТМЗ) $d = d_{отв}$;

c) for burners with partial premixing (type ГТ-50-800 ХТЗ) $d = d_{отв.ср}$.

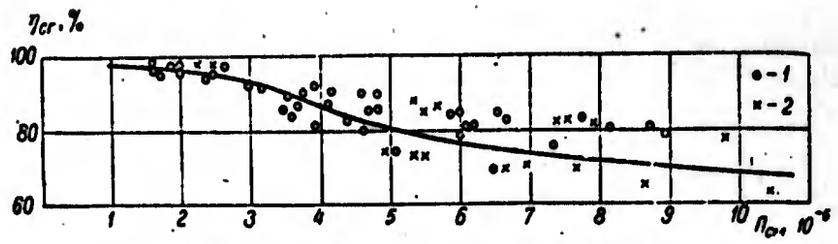

Fig. 56. Variation of combustion completeness with mixing parameter (burners with gas distribution through a slot; α_1 = 1,2—1,5; $t_в$ = 180—270° C; $t_{к.с}$ = 500—750° C; fuel is natural gas): 1) ГТН-9-750, $D_{п.т}$ = 1320 mm; 2) ГТ-25-700, $D_{п.т}$ = 1305 mm.

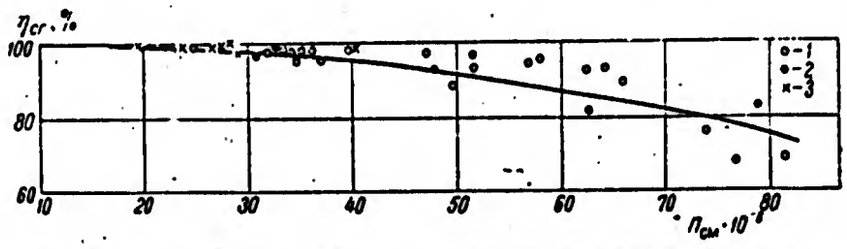

Fig. 57. Variation of combustion completeness with mixing parameter (burners with gas distribution through holes; α_1 = 1,2—1,4; $t_в$ = 170—270° C; $t_{к.с}$ = 670—750° C; fuel is city gas): 1) Block of chambers ГТ-100-750, $D_{п.т}$ = 270 mm; 2) ГТ-100-750, $D_{п.т}$ = 400 mm; 3) ГТУ-6-750, $D_{п.т}$ = 270 mm.

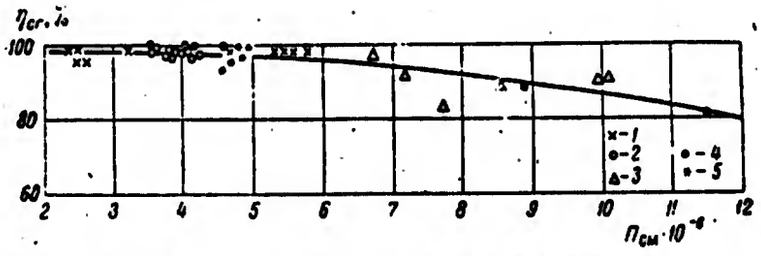

Fig. 58. Variation of combustion completeness with mixing parameter (burners with hollow vanes; α_1 = 1,25—2,5; $t_в$ = 100—300° C; $t_{к.с}$ = 400—700° C; fuel is natural gas): 1) ГТ-50-800 (experimental), $D_{п.т}$ = 905 mm; 2) ГТ-50-800 (КСВД), $D_{п.т}$ = 905 mm; 3) ГТ-50-800 (КСНД), $D_{п.т}$ = 1005 mm; 4) ГТН-9-750; 5 — ГТ-25-700 (I), experimental.

Figures 56, 57, and 58 present the generalized curves for combustion completeness versus mixing parameter for the three types of burners listed above. The experimental relationships are approximated by the equation

$$\eta_{cr} = \left(1 - e^{-\frac{B}{n_{см}}}\right) 100\%,$$

where the experimental constant B for each burner type has different values: B = 10 for burners with slot-type gas distribution (Fig. 56); B = 116 for burners with gas distribution through holes (Fig. 57);

B = 20 for burners with hollow vanes (Fig. 58). It should be noted that the relation $\eta_{cr}=f(\Pi_{cm})$. strictly speaking, is valid when the basic modeling conditions are satisfied. The curves presented correlate combustion chambers with similar construction of the burners and flametubes, operating in some range of the operating parameters (α, t_v). This explains the scatter of the experimental points for different combustion chambers relative to the average curve. Increased scatter is also the result of relative inaccuracy of the determination of the combustion completeness in the various chambers and particularly in the head sections.

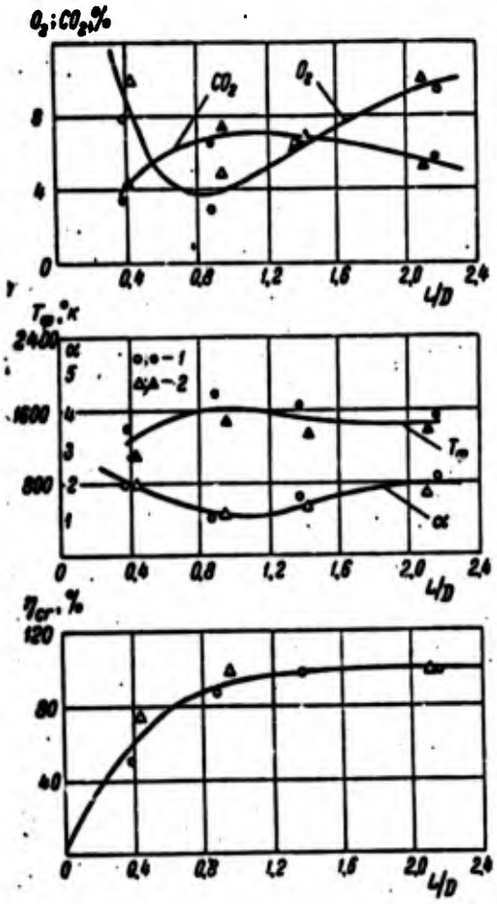

Fig. 59. Variation of oxygen concentration, carbon dioxide concentration, lame temperature, excess air and fuel combustion completeness along flametube length for two combustion chamber models ГТ-100-750 ЛМЗ (fuel is mixed gas): 1) Experiment No. 35; $D_{в.т}=400$; $\alpha_{общ}=6,38$; $\alpha_1=1,80$; $t_в=277$; $t_{ух}=747$; $p=1,39$; $U_p=4,92$; 2) Experiment No. 23; $D_{в.т}=370$; $\alpha_{общ}=5,48$; $\alpha_1=1,6$; $t_в=289$; $t_{ух}=735$; $p=1,41$; $U_p=5,88$.

Considering the above, we can consider that approximate hot-flow modeling for the burning of gaseous fuel in the case of diffusion combustion will be satisfied if the following conditions are met:

1) geometric similarity;

2) α_1, $\alpha_{общ}$, $t_в$=idem and the same fuel;

3) $\Pi_{см}$ = idem.

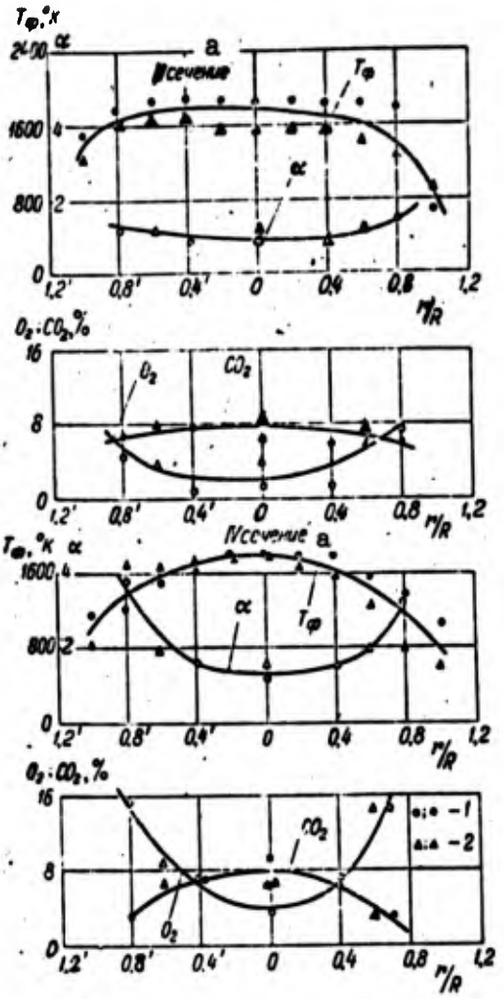

Fig. 60. Variation of flame temperature, excess air, oxygen concentration and carbon dioxide concentration along the radius for two combustion chamber models ГТ-100-750 ЛМЗ; 1) Experiment № 35: $D_{п.т}$ = 400 mm; 2) experiment No. 23; $D_{п.т}$ = 270 mm; a) Section.

As an example, Figs. 59 and 60 present the experimental curves for O_2 and CO_2 concentration, excess air and flame temperature distribution along the radius and length of a flametube, and also the variation of the combustion completeness along the length of two combustion chamber models ГТ-100-750 ЛМЗ with flametube diameters 400 and 270 mm, obtained with the modeling conditions mentioned above satisfied. The experimental points for the two models are grouped with slight scatter around common curves, which confirms the identity of the flame structure and combustion completeness for geometrically similar combustion chambers operating on gaseous fuel.

Table 7.4 presents the scheme and an example of the conversion of the combustion completeness obtained on a test model to a full-scale chamber operating in a GTE cycle.

TABLE 7.4

1 Наименование	2 Обозначение	3 Размерность	4 Формула	5 Пример расчета ГТ-100-750		
				$D_{п.т}$=270 модель 6	$D_{п.т}$=400 модель 6	$D_{п.т}$=400 натура 7
8 Давление в камере	P	ата	10 Из расчета схемы ГТУ	1,37	1,53	26,0
11 Диаметр регистра	$D_р$	м	12 Конструктивный расчет регистра	0,128	0,185	0,185
13 Диаметр пламенной трубы	$D_{п.т}$	м	14 Из теплового расчета камер сгорания	0,27	0,4	0,4
15 Относительная длина до сечения	l_x	—	$L_{ог}/D_{п.т}$	2,10	2,17	2,0
16 Характерный размер газового канала	d	м	$d = d_{отв}$	$2{,}1\cdot10^{-3}$	$3\cdot10^{-3}$	$3\cdot10^{-3}$
17 Средний расход газов до сечения	G_h	18 кг/ч	$G_р + G_ш + B_т$	2783	4831	43 800
19 Избыток воздуха в сечении	a_l	—	20 Из теплового расчета	2,35	2,3	2,3
21 Температура воздуха	$T_в$	°К	22 Из расчета схемы ГТУ	557	531	550
23 Температура факела	$T_ф$	°К	24 Из уравнения теплового баланса	1410	1415	1420
25 Удельный вес газов	$\gamma_г$	26 кг/м³	$\gamma_{ог}\frac{T_0}{T_ф}P$	0,347	0,347	6,54
27 Скорость воздуха на выходе из регистра	$w_р$	28 м/сек	29 Из гидравлического расчета	56,1	37,1	40,0
30 Скорость топливного газа на выходе из горелки	$w_г$	28 м/сек	31 Из расчета горелки	47,0	42,8	45,0
32 Характерная скорость	$w_{гор}$	28 м/сек	$\frac{a_l w_р + w_г}{a_l + 1}$	50	39,2	42,1
33 Параметр смешения	$\Pi_{см}$	—	$\frac{d^2 G_п \cdot 10^{-6}}{3600 \cdot w_{гор} \cdot D_р \gamma_г D_{п.т}^3 l_x}$	37,1	30,9	16,8
34 Полнота сгорания расчетная	$\eta_{сг}^{р}$	%	35 По кривой рис. 57	97,0	98,0	99,0
36 Полнота сгорания опытная	$\eta_{сг}^{оп}$	%	37 По опытным данным	98,0	99,0	—

1) Item; 2) symbol; 3) dimension; 4) formula; 5) calculation example; 6) model; 7) full scale; 8) chamber pressure; 9) [illegible]; 10) from analysis of GTE cycle; 11) register diameter; 12) register structural analysis; 13) flametube diameter; 14) from combustion chamber thermal analysis; 15) relative length up to section; 16) characteristic dimension of gas channel; 17) average gas flowrate up to section; 18) kg/h; 19) air excess at section; 20) from thermal analysis; 21) air temperature; 22) from GTE cycle analysis; 23) flame temperature; 24) from heat balance equation; 25) gas specific weight; 26) kg/m^3; 27) air velocity at register exit; 28) m/s; 29) from hydraulic analysis; 30) fuel gas velocity at burner exit; 31) from burner analysis; 32) characteristic velocity; 33) mixing parameter; 34) theoretical combustion completeness; 35) from curve of Fig. 57; 36) experimental combustion completeness; 37) from experimental data.

Manuscript Page No.	Transliterated Symbols
2	к.с = k.s = kamera sgoraniya = combustion chamber
2	т = t = teplovoy = thermal
2	гидр = gidr = gidravlicheskiy = hydraulic
2	з.к = z.k = za kamera = combustor exit
2	ст = st = staticheskiy = static
2	сг = sg = sgoraniye = combustion
3	ог = og = ognevoy = burning
3	п.т = p.t = plamennaya truba = flame tube
4	хим = khim = khimicheskiy = chemical
5	т = t = turbulentnyy = turbulent
5	исп = isp = ispareniye = vaporization
5	д = d = diffuzionnyy = diffusion
5	ф = f = fakel = flame
5	общ = obshch = obshchiy = total
5	в = v = vozdukh = air
5	гор = gor = goreniye = combustion
6	см = sm = smesheniye = mixing
6	пр = pr = prebyvaniye = flow

7 т = t = [not specifically identified]

7 к = k = [not specifically identified]

7 т = t = turbulentnyy = turbulent

7 м = m = molekulyarnyy = molecular

8 к = k = kaplya = droplet

8 ср = sr = srednyy = average

8 пл = pl = plamya = flame

8 г = g = gaz = gas

8 п = p = polnyy = total

11 п = p = par = vapor

15 ух = ukh = ukhodyashchiy = exit

15 пк = pk = [not specifically identified]

15 п.ф = p.f = [not specifically identified]

16 н.к = n.k = [not specifically identified]

16 н.ф = n.f = [not specifically identified]

18 н = n = nizhnyy = lower

18 вн = vn = vnesennyy = introduced

18 р = r = raschetnyy = theoretical

18 оп = op = opytnyy = experimental

18 щ = shch = shchel' = slot

18 р = r = registr = register

18 т = t = toplivo = fuel

18 л = l = lopast = vane

18 вых = vykh = vykhod = exit

18 к = k = kislorod = oxygen

18 гор = gor = goreniye = combustion

19 ст = st = staticheskiy = static

22 м = m = maksimal'nyy = maximal

23 к = k = kipeniye = boiling

23 и = i = ispareniye = vaporization

23 в = v = vosplameneniye = ignition

24 к = k = konus = cone

28 отв = otv = otverstiye = hole

28 ср = sr = srednyy = average